Deep Mining 2017: Eighth International Conference on Deep and High Stress Mining – J Wesseloo (ed.)

doi:10.36487/ACG_rep/1704_04_Kalenchuk

Large-magnitude seismicity at the Westwood mine, Quebec, Canada

KS Kalenchuk *Mine Design Engineering, Canada*

R Mercer *Knight Piésold Ltd, Canada*

E Williams *Iamgold, Canada*

Abstract

The Westwood mine is located approximately 40 km east of the town of Rouyn-Noranda and 80 km west of the town of Val-d'Or in Quebec, Canada. Operations at the Westwood mine were halted by three large-magnitude seismic events which occurred over two days in May, 2015. This paper provides an overview of the seismic events and summarises the numerical back-analyses completed using global mine-scale and local drift-scale models, to gain an understanding of the mechanisms that fundamentally contributed to what was considered, by a review panel of experts, to be an unforeseen series of events. A global mine model was required to provide a reasonable estimate of the induced stresses on nearfield pillars and excavations and a detailed small-scale model was necessary to adequately capture the failure mechanisms in drift ribs, which played a role in sublevel pillar performance. The global model did not provide sufficient resolution to capture drift-scale mechanisms. While the local model was insufficient for calibration of the mine system boundary conditions, the combination of global and local models is valuable in defining mine-scale stress conditions and their impact on local, drift-scale failure mechanisms.

Keywords: *numerical modelling, pillar stability, rockbursting*

1 Introduction

The Westwood mine is located approximately 40 km east of the town of Rouyn-Noranda and 80 km west of the town of Val-d'Or in Quebec, Canada (Figure 1). The mine is located on the eastern part of the Doyon Division mining property. Gold production at the Westwood mine started in March, 2013 and the first ingot was poured on March 27, 2013. The official commercial production started on July 1, 2014.

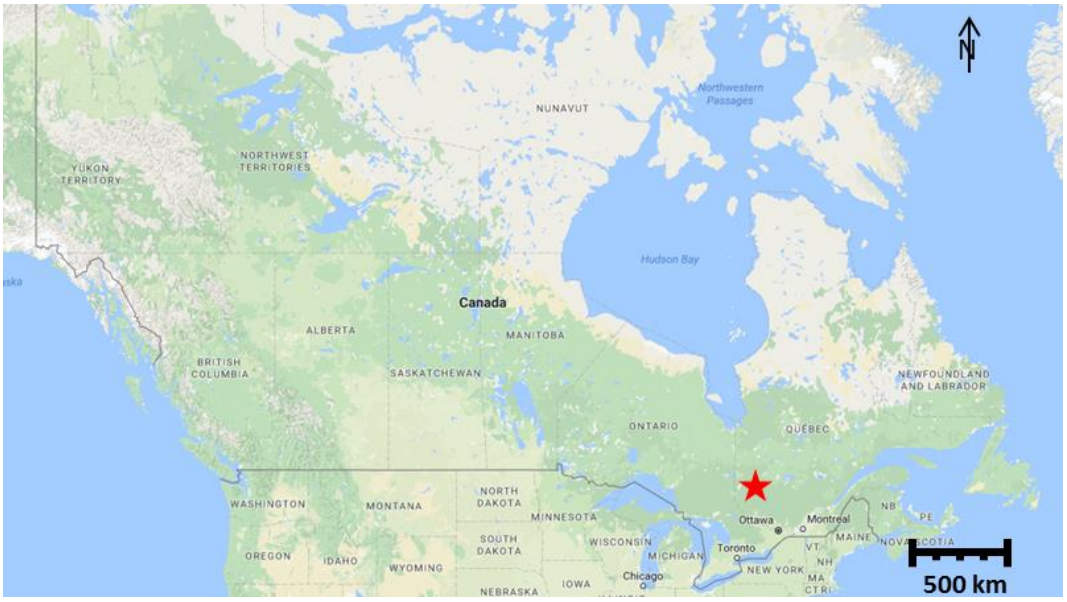

Figure 1 Westwood mine location (red star) within the province of Quebec, Canada

Production in the 104-mining block in Zone 2 of the Westwood mine was halted by three large-magnitude seismic events over two days in May 2015. At 3:28 AM on 25 May 2015 a M_N3.2 event occurred near the 104-06 sublevel, this was followed shortly after by a M_N2.7 event at 3:38 AM near the 104-03 sublevel. Damage occurred on all sublevels from 104-02 to 104-10 (note that there is no 104-05), although the main ramp was not affected. Significant falls of ground occurred on 104-02, 104-03 and 104-06, with 104-04 being inaccessible for inspection. No miners were injured, and all levels in the 104 horizon were immediately closed. More than 40 hours later, on 27 May 2015 at 8:11 PM, a M_N2.4 event occurred near the 104-10 sublevel, with no further damage detected. Mining activities leading up to these events were reviewed and no specific blast (production or development) could be identified as an obvious trigger. Figure 2 illustrates the locations of the three large-magnitude events relative to the central infrastructure corridor (CIC). The CIC includes the central ramp connection to each of the subs and sublevel development in proximity to the ramp. Infrastructure development is situated in the orebody footwall.

This paper provides an overview of the seismic events and summarises the numerical back-analyses completed using global mine-scale and local drift-scale models, to gain an understanding of the mechanisms that fundamentally contributed to what was considered, by a review panel of experts, to be an unforeseen series of events.

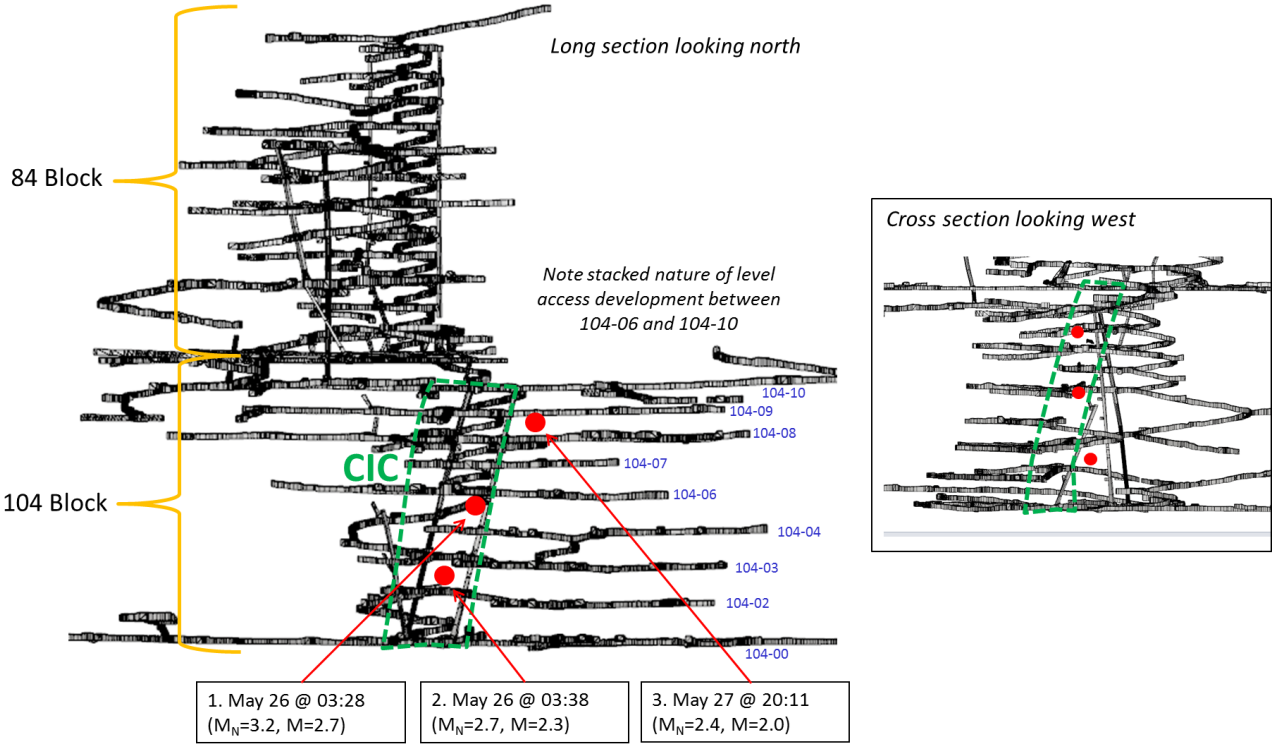

Figure 2 104 mining block geometry and location of May 2015 large-magnitude events

2 Geological setting

The Westwood mine is part of the Doyon-Bousquet-Laronde mining camp, which is located within the Southern Volcanic Zone of the Abitibi sub-province. Figure 3 provides a geological cross-section of the Westwood property. Zone 2 of the Westwood deposit is hosted in felsic volcanic rock with sub-vertical to steeply south dipping schistosity. Schistocity is heterogeneous and varies in intensity from moderate to strong. East–west anastomosing high-strain corridors are observed throughout the property. Major fault structures are present in the mine vicinity, however, these features did not directly contribute to the seismic events of interest to this study and so will not be discussed further.

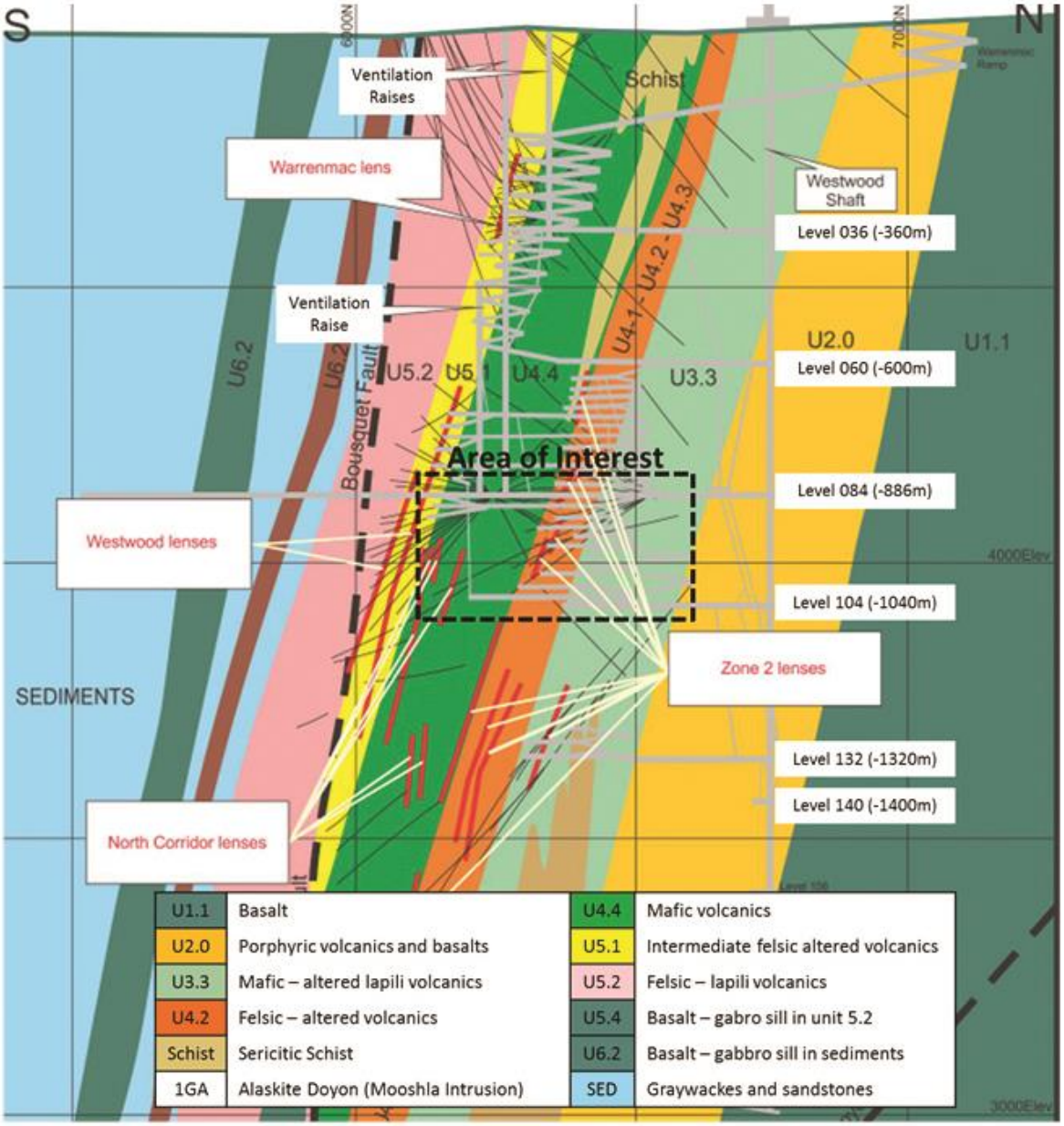

U3 is a very complex mafic-intermediate unit (basaltic to andesitic). The U3 varies from massive to strongly foliated in an imbricating fashion. Rock mass quality within the U3 is particularly unpredictable due to the complex alternation between competent and strongly altered/foliated portions of the rock mass as well as a pervasive epidote alteration that mimics silicification.
U4 is a felsic rhyodacite which is the main host rock of the Zone 2 extension orezones. This unit characterised by very intense foliation.
U5 is a mafic-intermediate unit (basaltic to andesitic) which hosts some of the Zone 2 extension orezones.

Figure 3 Cross-section showing major lithologies relative to mine workings and the area influenced by May 2015 seismicity

3 Geotechnical site characterisation

Intact rock properties have been defined for this study, based on laboratory data provided by Simon (2009). Parameters for the lithological units relevant to the back-analysis of May 2015 seismicity are summarised in Figure 4 and Table 1. Rock mass classification parameters (Table 2) were taken from previous analyses of geotechnical data provided by Leber et al. (2015). In this study, reasonable upper and lower bound strength criterion parameters were selected as a starting point for model calibration.

Table 1 Summary of intact material properties

Unit	Density (10^3kg/m^3)	E_i (GPa)	v	Upper bound			Parallel to foliations		
				UCS (MPa)	m_i	Tensile strength (MPa)	UCS (MPa)	m_i	Tensile strength (MPa)
U3	2.9	81	0.3	154	10	13.3	120	6	21.9
U4	2.83	49	0.2	104	10	10.0	90	7	12.6
U5	2.87	69	0.24	169	13	11.5	13.5	8	18.5

Table 2 Summary of rock mass classification (GSI)

Unit	GSI
U3	62 ± 8
U4	54 ± 12
U5	52 ± 12

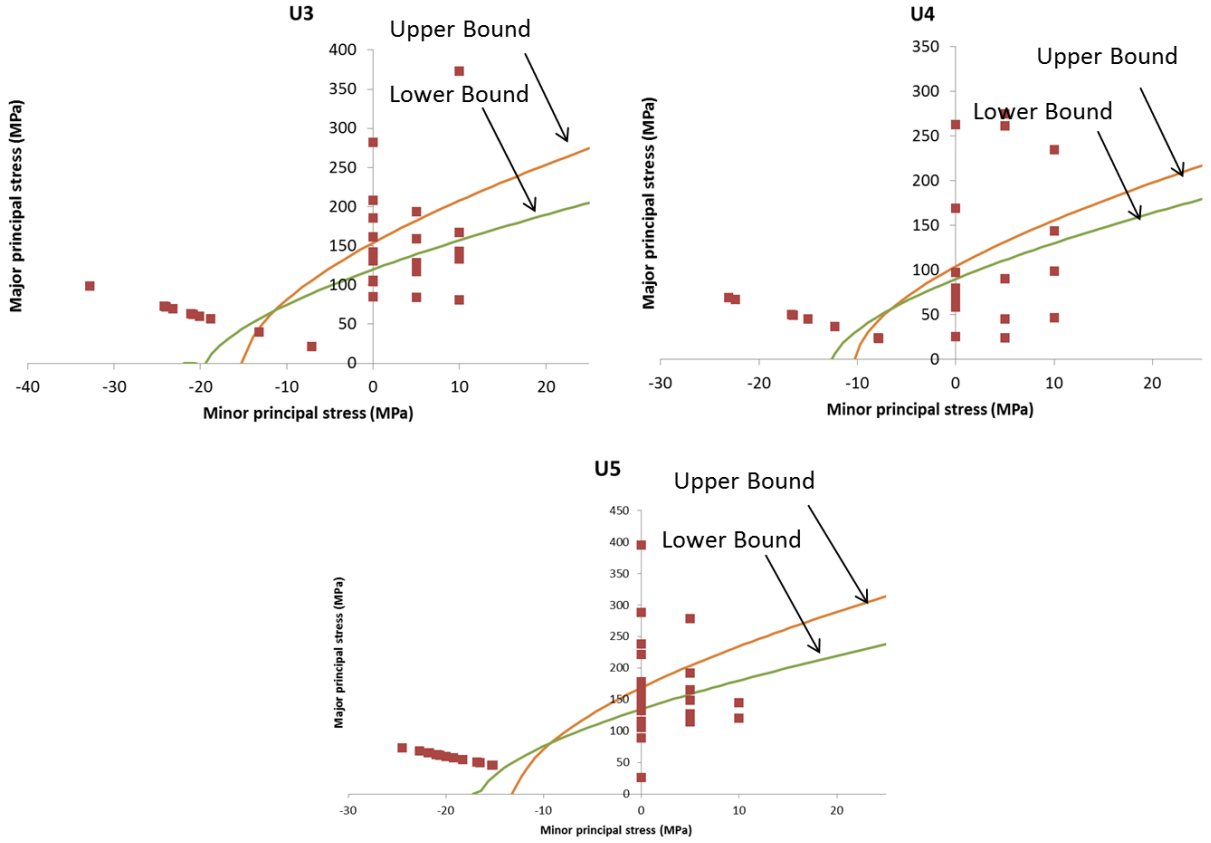

Figure 4 Intact material properties

4 Numerical back-analysis

The main objective of the numerical analyses performed in this study was to improve the understanding of overall rock mass behaviour in Zone 2 at the Westwood mine and to better define the factors that contributed to the generation of the observed seismicity. To achieve this, a numerical model was developed and calibrated with a combination of the available seismic data (from between November 2013 and June 2015), underground observations, the condition of boreholes, and inspection of the available

core. The global model was developed using FLAC3D and included all development and stoping geometries in the relevant mining blocks. Geotechnical domains were explicitly defined in order to adequately capture the influence of variable material properties across lithological boundaries.

4.1 Summary of calibration data

4.1.1 Seismic data

Micro-seismic data was utilised to identify regions that could be deemed to be yielded (aseismic) or transitioning through the yield process (seismically active). One of the main conclusions from the seismic data analysis, corroborated by damage observations made underground, was that the CIC above 104-06 was a stress reduced area and that stresses had been re-distributed to the surrounding seismically active regions (Figure 5) prior to the May 2015 events. After the May 2015 events, the available data suggests that the stress reduced area extended downwards to approximately 104-03.

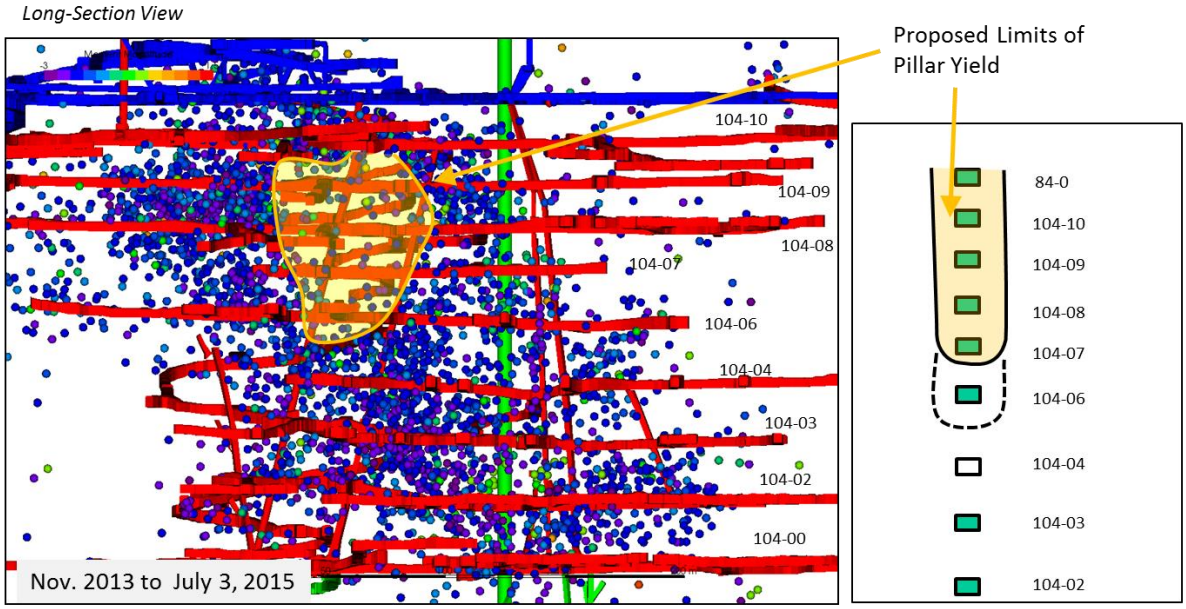

Figure 5 Interpretation of the extent of rock mass yield based on aseismic zones identified in seismic data

4.1.2 Probe hole observations

Two series of probe holes were drilled during the geomechanical site investigation following the May 2015 seismicity. The first series was comprised of 35 holes drilled in the 104-09/10 pillar to evaluate the state of the pillar. Borehole camera observations focussed on assessing the condition of the drillhole walls (fracturing, breakout, squeezing). Holes were progressively drilled from east to west approaching the central 'yielded' zone as identified by the spatial distribution of the induced seismicity. Figure 6 provides a summary of the interpreted rock mass conditions based on drillhole observations, as well as the corresponding seismic record in the same area. The results from this series of drillholes support the seismic assessment and identified the transitions between the no damage zone (relatively low stress) and the yielding zone (relatively high stress), and between the yielding zone and the highly fractured aseismic zone (residual load).

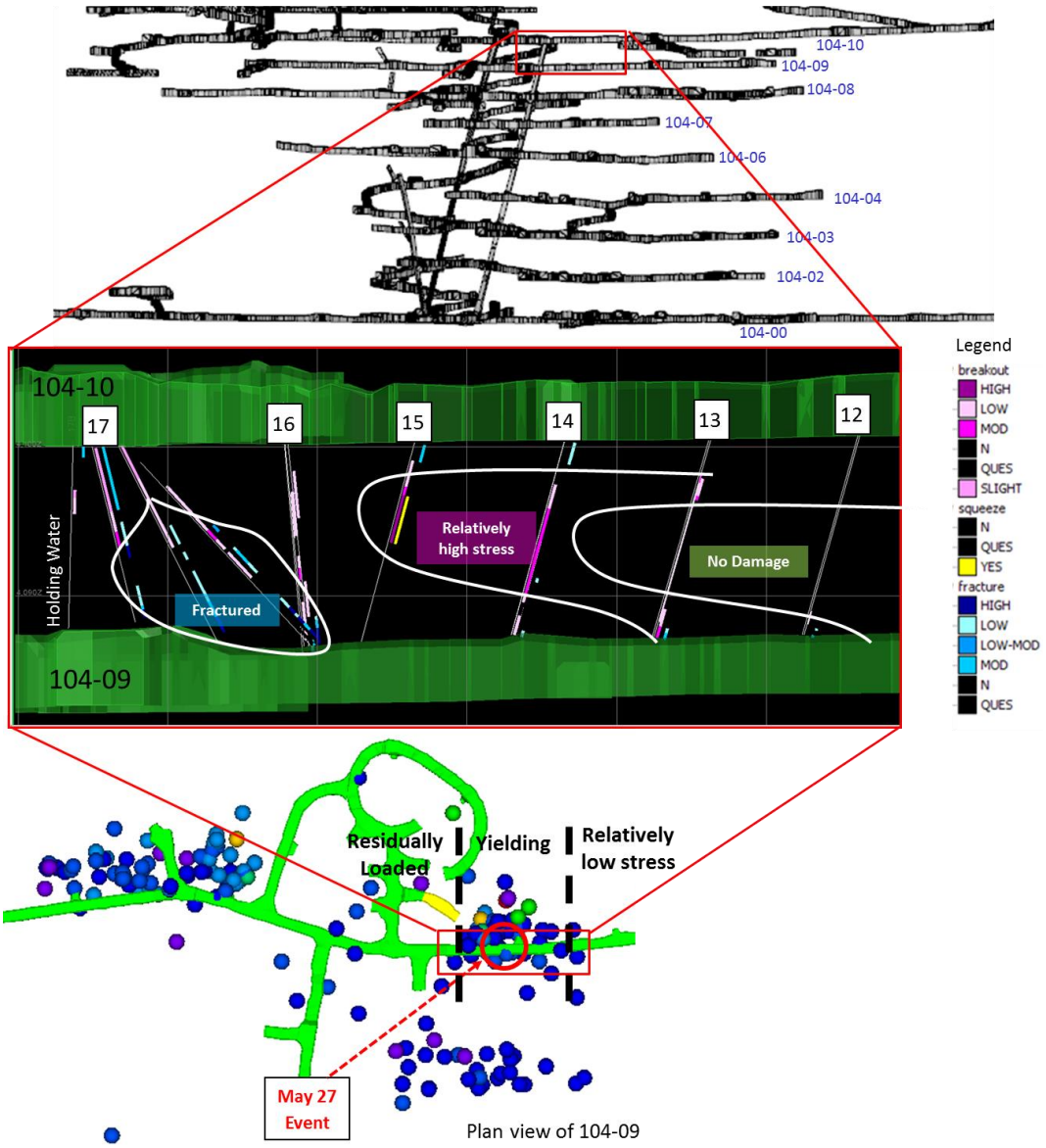

(top) Long section looking north showing the locations of test hole drilling through the pillar between 104-09 and 104-10
(center) Interpretation of test hole observations (driller notes and borehole camera surveys) showing zones of no damage, high stress and fractured ground
(bottom) test hole area showing aseismic zone (residual load), seismic activity (high stress) and low seismicity (low stress)

Figure 6 104-09/10 probe holes

The second series of holes were comprised of two drillholes (between 90 and 100 m long) that were drilled to evaluate (by core inspection and borehole camera) the state of the 104-06 and 104-03 pillars and to investigate whether there were any previously undetected large-scale structural features (Figure 7). No

large-scale shears or faults where encountered and core conditions varied between zones of intense fracturing (mixed disking, disturbed foliation, and apparent stress damage) and competent zones. Borehole camera surveys were also completed and it was concluded that the borehole walls were generally less fractured than the core.

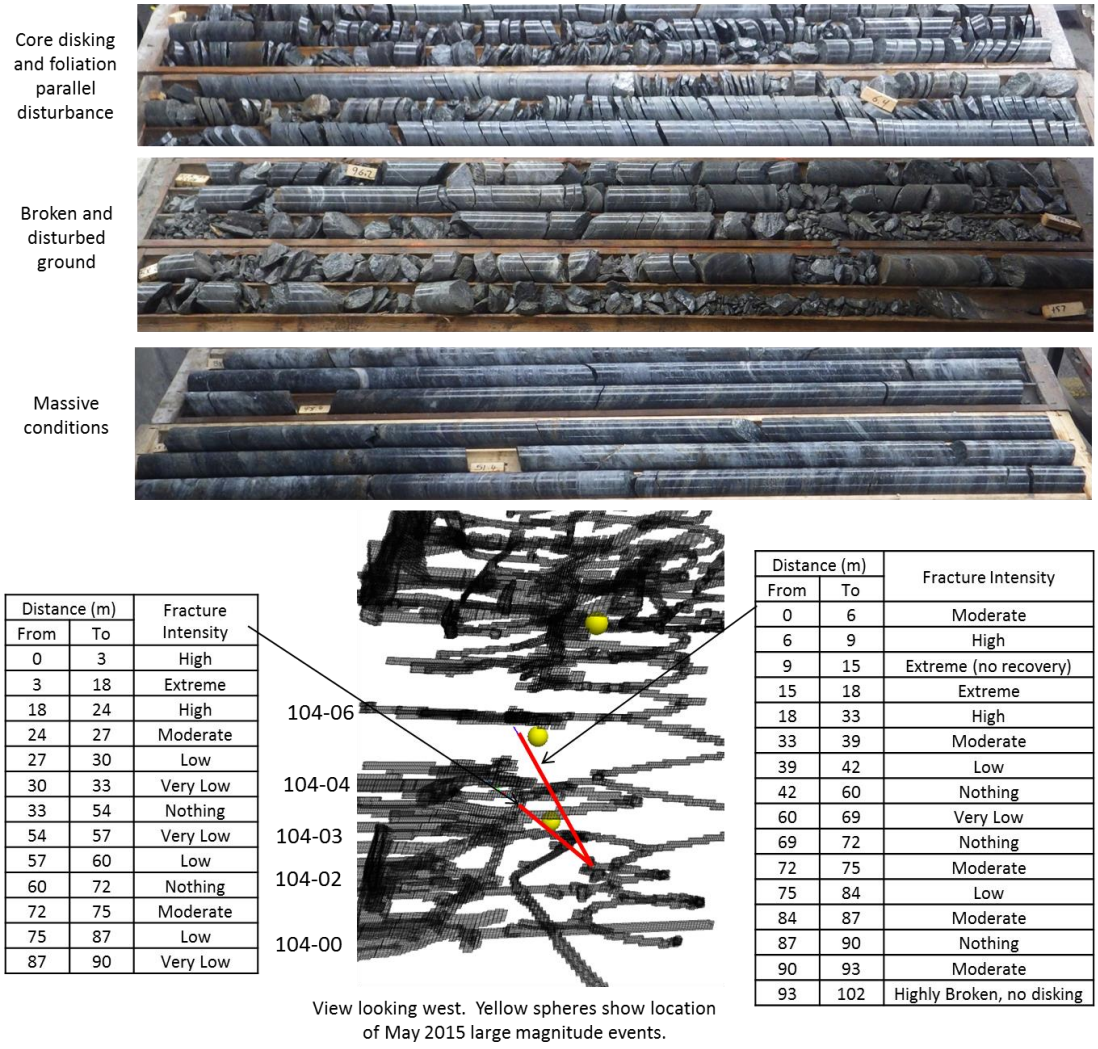

Distance (m)		Fracture Intensity
From	To	
0	3	High
3	18	Extreme
18	24	High
24	27	Moderate
27	30	Low
30	33	Very Low
33	54	Nothing
54	57	Very Low
57	60	Low
60	72	Nothing
72	75	Moderate
75	87	Low
87	90	Very Low

Distance (m)		Fracture Intensity
From	To	
0	6	Moderate
6	9	High
9	15	Extreme (no recovery)
15	18	Extreme
18	33	High
33	39	Moderate
39	42	Low
42	60	Nothing
60	69	Very Low
69	72	Nothing
72	75	Moderate
75	84	Low
84	87	Moderate
87	90	Nothing
90	93	Moderate
93	102	Highly Broken, no disking

Figure 7 104-06 and 104-03 probe holes

4.1.3 Additional calibration data

Additional sources of calibration data included:

- Three borehole extensometers located on 104-10 and 104-08. The extensometer results suggested plastic rock mass behaviour, but the transition from elastic to plastic behaviour could not be identified with confidence. As such, it was difficult to draw quantitative conclusions from the extensometer results.
- Falls of ground in the CIC were documented in late 2013. The depth of failure measured for these falls of ground was utilised qualitatively to support the calibration model.

4.2 Model calibration

The first iteration of numerical simulations focussed on narrowing down the range of possible stress tensors and material property combinations. Corthesy et al. (1998) provides a comprehensive summary of in situ stress testing results for the Val-d'Or and Rouyn-Noranda region. From the available data, a range of possible stress states were defined and the results are summarised in Table 3.

Table 3 In situ stress tensors (ranges of magnitude and orientation) utilised during numerical model calibration (bold indicates the base case considered to be the most probable according to the available data)

Principal stress	Magnitude	Orientation (trend/plunge)
σ_1	(1.9, **2.5** or 2.8) × σ_3	000°/00°, **035°/00°** or 055°/00°
σ_2	(1.5, **1.7** or 1.9) × σ_3	090°/00°, **125°/00°** or 145°/00°
σ_3	**σ_v**	**000°/90°**

4.2.1 Far-field stress tensor

The only physical observation that was available at the time of the study, which provided insight into the potential stress tensor, was borehole squeezing observed in the 104-09/10 pillar probe holes (Figure 8). Squeezing of the probe holes suggested that the local major principal stress is slightly east of north at N15E. Numerical modelling results suggested that the local stress direction was relatively insensitive to the orientation of the far field stress tensor. This is due to the local excavation geometry, specifically that the stacked level development in the 104 block above 104-06 creates long (on strike) and thin pillars. A parametric analysis with the FLAC3D model suggested that the orientation of the local stress tensor within those pillars was not sensitive to far field azimuths varying from N00E to N50E (Figure 8). However, the local stress tensor magnitude was found to be sensitive to the far field orientation. For similar k-ratios, a N00E σ_1 azimuth results in higher major principal stresses in the pillars than a N55E σ_1 azimuth.

The lower levels in the 104 block (below 104-06) have not been geometrically stacked in the same fashion as those levels above 104-06. Here, the orientation of the local stress tensor is more sensitive to far field orientation. The pillars between the subs within the lower part of the CIC do not induce a significant rotation of the far field principal stress towards N00E.

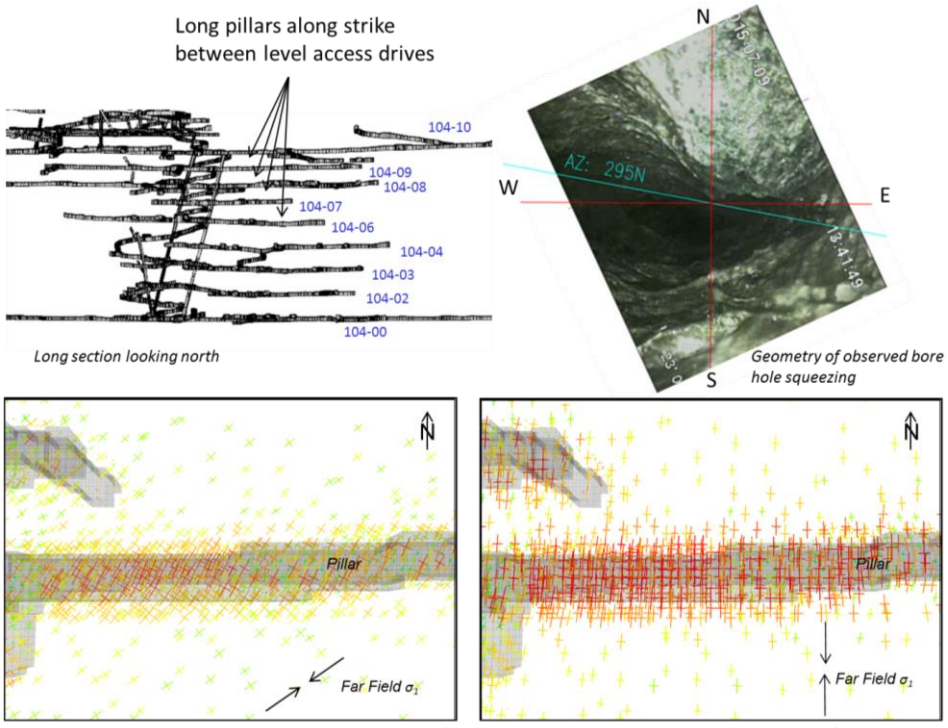

Figure 8 Rotation of far field stress tensor through pillars between sublevels above 104-06. Note that the simulated stress tensors within the pillar are very similar (roughly N–S major principal stress), despite varying far field orientations

4.2.2 Constitutive model

The model calibration process evaluated the influence of the assumed constitutive model, investigating both the role of anisotropy as well as the impact of post peak strain softening to the predicted pillar performance. It is interesting to note that pillar performance in the global model above 104-06 showed negligible response to isotropic versus anisotropic constitutive behaviour. It is clear that the rock mass is strongly anisotropic, however, due to the direction of loading (roughly perpendicular to schistosity) the inclusion of ubiquitous jointing (UJ) in the FLAC3D model yielded very similar results to the isotropic model. This result is due to both models having nearly identical strength in the direction perpendicular to the foliation.

4.2.3 Mine geometry

During preliminary model calibration, it was determined that it was necessary to utilise either excessively high far field stress magnitudes or unrealistically low material properties to generate sufficient yield through the rock mass to approximate the spatial extent of the previously defined stress-reduced region. This suggested that some component of the fundamental mechanisms contributing to pillar deterioration was not accounted for in the numerical representation of Zone 2 geomechanical rock mass behaviour.

Rib damage is commonly observed at the Westwood mine. In the area of interest, the severity of rib damage varies locally within the U3 depending on the intensity of foliation. Development drives orientated parallel to foliation (E–W) incur rib damage due to squeezing, a mechanisms that is well documented in the Val D'Or area (e.g. Mercier-Langevin & Hadjigeorgiou 2011; Potvin & Hadjigeorgiou 2008). Early numerical modelling had focussed on a global mine model to investigate the stress path and damage accumulation within the pillars left between level access development. As the rockburst investigation evolved, it was hypothesised that deformations in the development ribs was contributing to a wider effective span in drifts orientated parallel to the foliation. The wider effective span was influencing pillar performance by increasing the width to height ratio and, therefore, reducing confinement (σ_3) within the pillars, this concept is illustrated schematically by the simple two-dimensional model depicted in Figure 9.

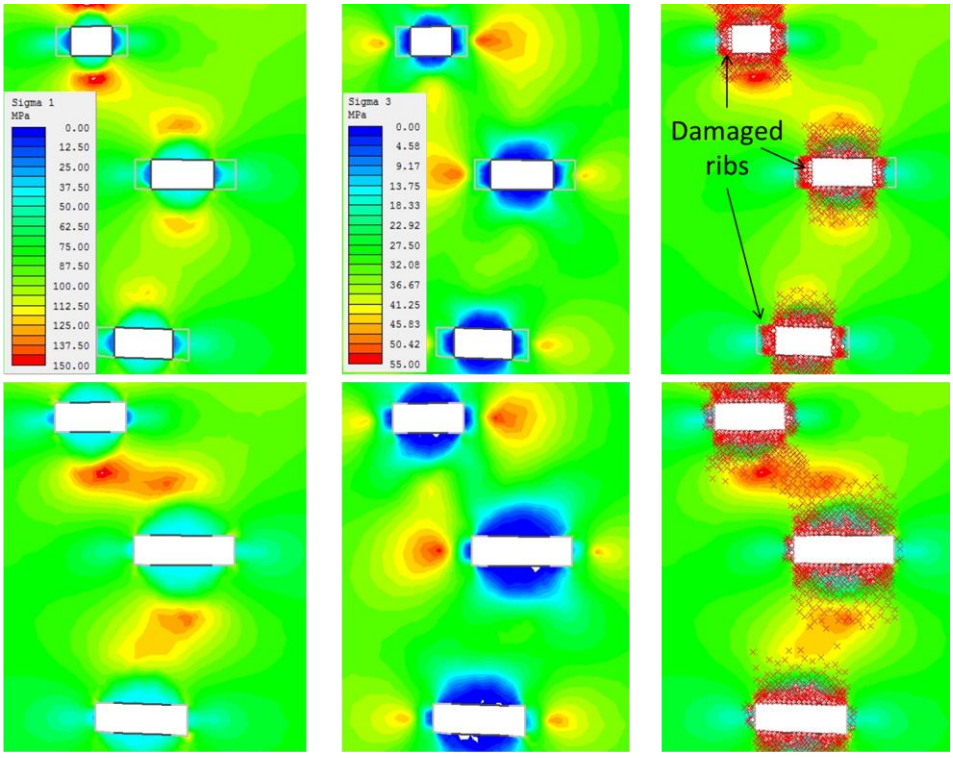

Simplified 2 dimensional simulations (Phase2) to demonstrate the influence of effective spans on pillar condition.
From left to right: σ1, σ3, yielded elements; Top: As built spans, Bottom: widened effective spans

Figure 9 Influence of widened effective span on pillar stability

The global mine model was of too coarse a resolution to investigate the reasonable extent of rib damage at the drift scale. As such, complementary local simulations were utilised to provide an estimate of the depth of damage. The geometric influence of damaged ribs was then incorporated into the three-dimensional model calibrations by explicitly adjusting the geometry of drifts orientated parallel to foliation to be consistent with wider effective spans. In the absence of quantitative data to support the post peak parameterisation of severely damaged ribs, the estimated damage volumes were completely extracted in the global numerical models. This approach to simulation of the effective span increase presents an extreme strain softening case. In reality, it would be reasonable to expect that drift ribs would retain some residual strength and stiffness. These residual parameters, and their true time dependency, are difficult to estimate in the absence of extensive instrumentation data.

With the inclusion of effective span geometries in the 104 mining block, model calibration has been achieved with more realistic far field stress magnitudes and material properties. The final far-field stresses and material strengths fall within the reasonable bounds based on the available data.

4.3 Final model results

At the completion of the model calibration work it became evident that a number of combinations of boundary conditions and material strengths could reproduce similar volumes of yielded rock mass and similar redistributions of stress around those volumes. These alternatives are summarised in Table 4. In any numerical modelling application, multiple combinations of input parameters and boundary conditions can produce similar conclusions and so, practitioners must be careful when concluding that any one simulation represents a unique and final answer. Figures 10 and 11 demonstrate how well the numerically predicted stress magnitudes and yield volumes correlate with the qualitative calibration data. Figure 10 demonstrates that observations made in a probe hole drilled near 104-06 and 104-03, can be directly correlated with numerical results. Broken ground was encountered in the probe holes in regions where numerical simulations produced yield. Intense disking was observed in core for regions where the simulations indicated high stress loading. Undisturbed ground was encountered in the probe holes for the same regions as where numerical results showed low stress conditions. Figure 11 demonstrates good agreement between numerical results and observations made by probe holes in the 104-09/10 pillar, observed broken ground correlates with yielded elements and borehole squeezing correlates with high stress conditions.

Table 4 Summary of best fit combinations of stress and strength based on model calibration

				Parameterisation				
					Perpendicular to foliations		Parallel to foliations	
Constitutive model	**Geometry model**	**K (σ_1:σ_3)**	**σ_1 trend**	**Unit**	**GSI**	**UCS (MPa)**	**GSI**	**UCS (MPa)**
UJ	As-built	2.8	055°	U3	62	135	54	120
				U4	54	90	42	90
				U5	52	150	40	135
UJ	Widened effective span	2.8	055°	U3	62	145	54	120
				U4	54	100	42	90
				U5	52	160	40	145
UJ	Widened effective span	2.5	055°	U3	62	135	54	120
				U4	54	90	42	90
				U5	52	150	40	145

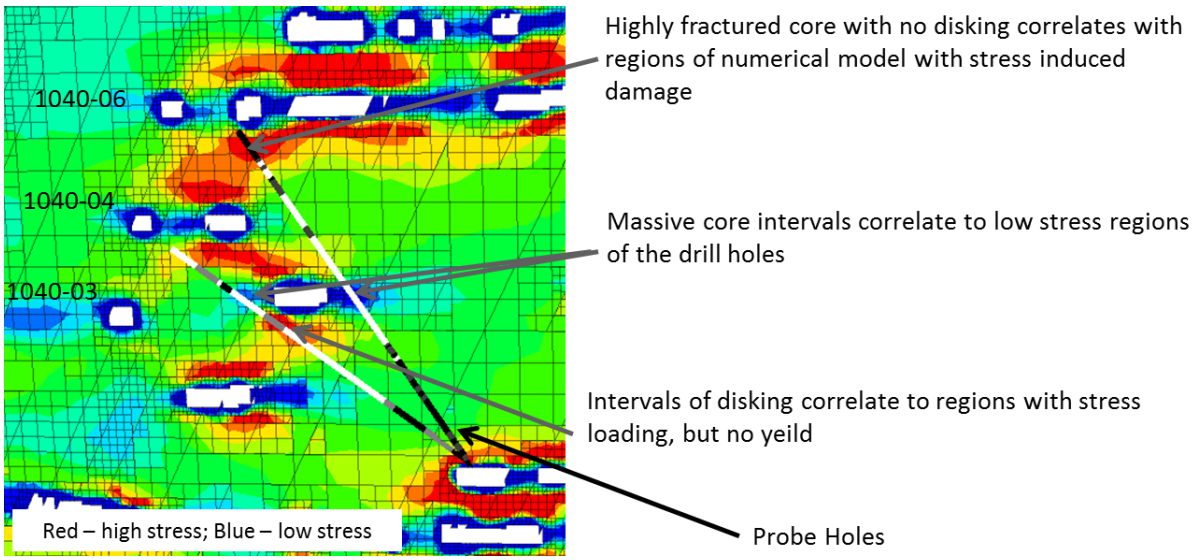

Figure 10 Comparison of model results to 104-06 and 104-03 probe holes

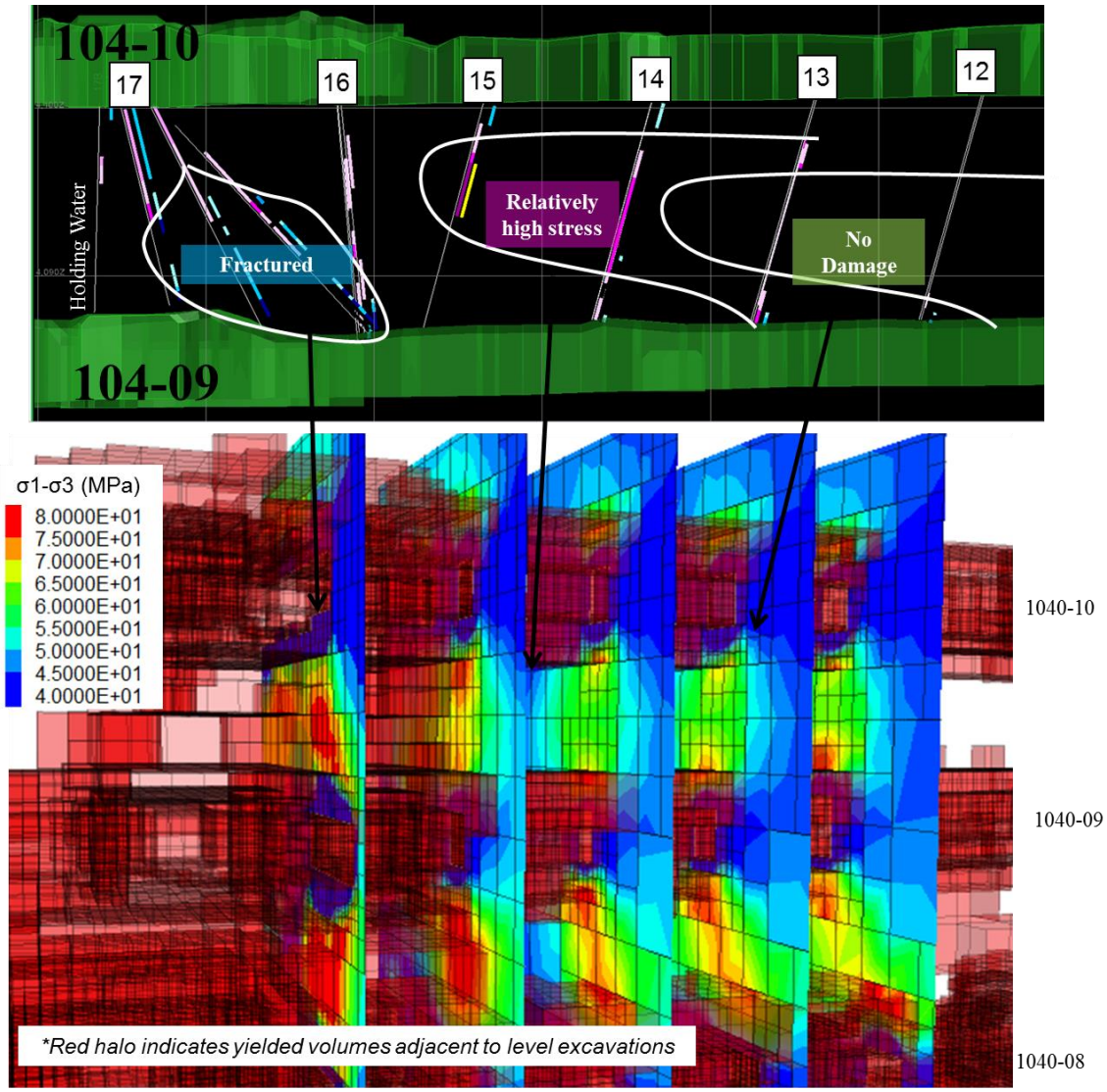

Figure 11 Comparison of model results to 104-09/10 probe holes

5 Discussion

It was concluded that the May 2015 seismicity was most consistent with a pillar bursting mechanism. Figure 12 illustrates the numerically reproduced progression of stress concentrations in the area of the M_N3.2 event. These seismic events, considered by the Rock Burst Review committee panel of experts to be unforeseen, ultimately occurred due to a complex series of factors including complex geological conditions, a unique mine geometry and a phenomena whereby rib deterioration resulted in a time-dependent increase in pillar aspect ratio and the associated deconfinement. The time dependency of rib deterioration provides a likely explanation for why the large-magnitude events did not appear to be temporally or spatially attributable to any specific blast.

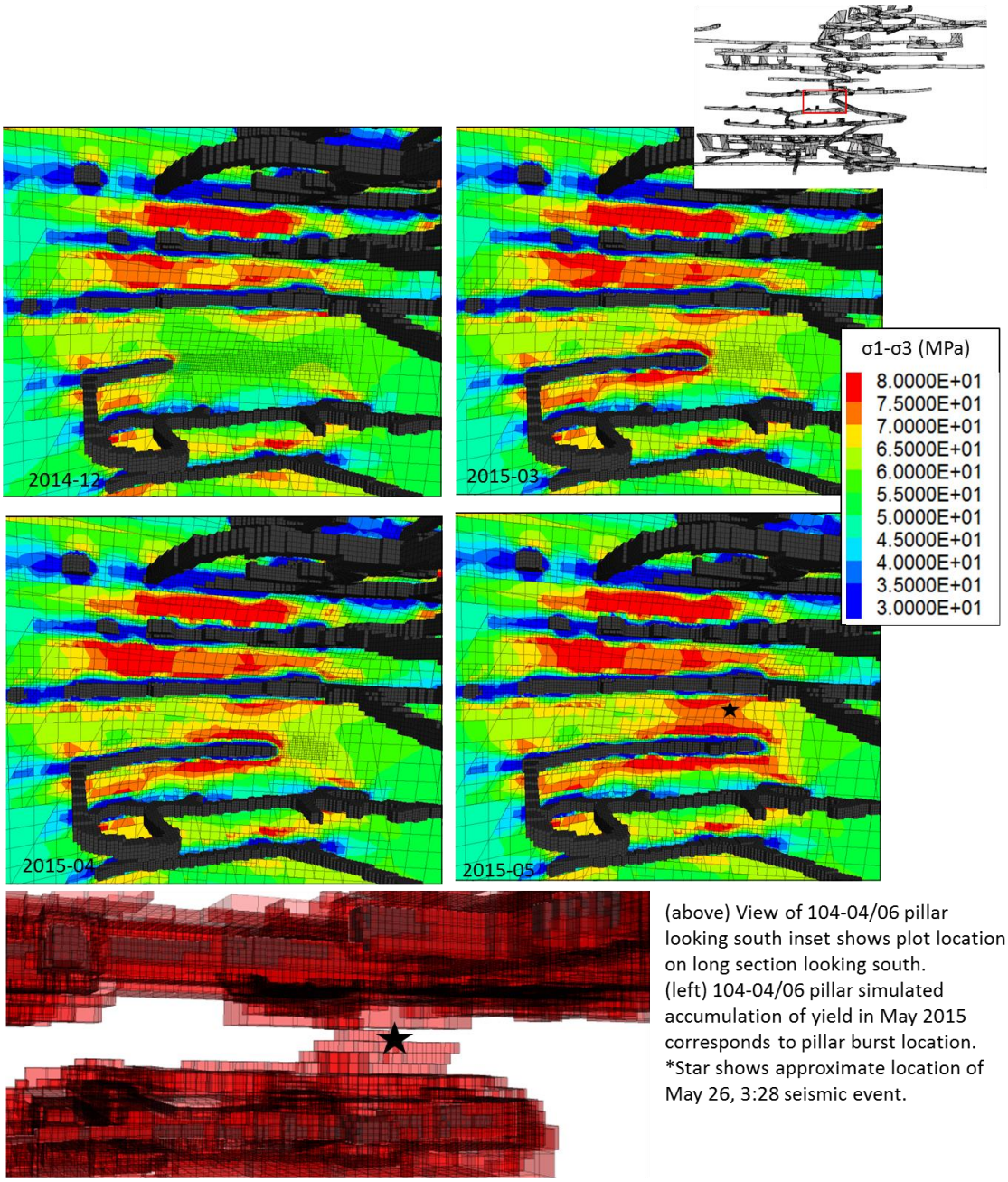

(above) View of 104-04/06 pillar looking south inset shows plot location on long section looking south.
(left) 104-04/06 pillar simulated accumulation of yield in May 2015 corresponds to pillar burst location.
*Star shows approximate location of May 26, 3:28 seismic event.

Figure 12 Evolution of numerically predicted stresses leading up to the M_N3.2 event and numerically predicted pillar yield

6 Conclusion

This study demonstrates the role of geometry in model calibration. Excavation geometry is commonly oversimplified, particularly in global, mine-scale models. In many cases, the simplification of excavation geometries in large-scale models may be acceptable, however, the decision to simplify void shapes, much like the decisions around constitutive models and material properties, must always be investigated and proven to be appropriate given the objectives of the modelling exercise. In this study, a global mine model was required to provide a reasonable estimate of the induced stresses on nearfield pillars and excavations and a detailed small-scale model was necessary to adequately capture the failure mechanisms in drift ribs, which played a role in sublevel pillar performance. The global model did not provide sufficient resolution to capture drift-scale mechanisms. While the local model was insufficient for calibration of the mine system boundary conditions, the combination of global and local models is valuable in defining mine-scale stress conditions and their impact on local, drift-scale failure mechanisms.

This study also found that multiple combinations of input parameters can yield similar conclusions and so, practitioners must be careful when concluding that the completed simulations represent a unique and final answer. In the current study, the preliminary models would have resulted in the use of excessively high far field stress or unrealistically low material properties, both of which produced acceptable volumes of yield and imposed reasonable stress increases in seismically active areas of the mine. However, the use of these 'miss-calibrated' models would have led to incorrect engineering design guidelines for the Westwood mine and impacted future mine planning.

Acknowledgement

The authors would like to thank Iamgold for permission to publish this case study.

References

Corthesy, R, Gill, DE & Leite, MH 1998, 'Elaboration d'un modele de prediction des constraints in-situ dans la region de la faille de Cadillac', *CIM Bulletin,* vol. 91, no. 1,020, pp. 54–58.

Leber, R, Morel, R, Williams, E & Deshaies, M 2015, *Westwood Mine Quebec, Canada NI-43-101 Technical Report Mineral Resource and Reserve Estimate as of December 31st 2014*, report prepared for Iamgold Corporation.

Mercier-Langevin, F & Hadjigeorgiou, J 2011, 'Towards a better understanding of squeezing potential in hard rock mines', *Mining Technology*, vol. 120, no. 1, pp. 36–44.

Potvin, Y & Hadjigeorgiou, J, 2008, 'Ground support strategies to control large deformations in mining excavations', *Journal of the Southern African Institute of Mining and Metallurgy*, vol. 108, pp. 393–400.

Simon, R 2009, *Essais de Laboratoire, Projet Westwood*, report prepared for Gestion Iamgold Quebec Inc.